Journal of Advanced Marine Engineering and Technology, Vol. 48, No. 6, pp. 414~420, 2024
J. Advanced Marine Engineering and Technology (JAMET)
https://doi.org/10.5916/jamet.2024.48.6.414

ISSN 2234-7925 (Print)
ISSN 2765-4796 (Online)
Original Paper

Analysis of overtopping wave energy converters with ramp angle variations using particle-based simulation

Sung-Hwan An[1] · Jong-Hyun Lee[†]

(Received December 5, 2024 ; Revised December 16, 2024 ; Accepted December 22, 2024)

Abstract: An overtopping wave energy converter (OWEC) is designed to convert the kinetic and potential energies of overtopped waves into electricity. The performance of OWEC is closely influenced by wave characteristics such as wave height and period, underscoring the importance of optimizing their design for specific marine environments. This study utilized marine environmental data from the coastal region of Ulleung-eup and conducted numerical simulations using the smoothed particle hydrodynamics method to analyze the overtopping performance of an OWEC under varying design parameters. Four models with different ramp configurations are proposed and evaluated. The hydraulic efficiency, derived from the overtopped flow rate, was used to assess and compare the performance of each model. Among the designs, the model with a ramp angle of 35° demonstrated the best performance. This study offers valuable insights into the optimal ramp design of OWEC for specific marine conditions and emphasizes the need for future studies incorporating three-dimensional simulations and experimental validation.

Keywords: Overtopping wave energy converter, Energy efficiency, Smoothed Particle Hydrodynamics, 2D numerical simulation, Ramp angle

1. Introduction

With increasing concerns about environmental issues and the need to transition from fossil fuels to renewable energy sources, various methods for renewable-energy-based power generation, such as solar photovoltaics, solar thermal energy, hydropower, ocean energy, geothermal energy, and bioenergy, have gained attention. In South Korea, the proportion of energy derived from renewable sources is relatively low, at 5.21%, with marine energy accounting for only 0.6%. However, given South Korea's geographic characteristics, its proximity to the ocean presents substantial potential, with an estimated 18,000 MW of marine energy available, including tidal (6,500 MW), wave (1,000 MW), and ocean thermal (4,000 MW) energy.

Wave energy converters can be categorized into oscillating body types, which directly convert the kinetic energy of waves into electricity; oscillating water column types, which generate power by converting the airflow energy caused by wave-induced oscillations into turbine motion; and overtopping types, which transform the energy of overtopped waves into potential energy to drive turbines.

In overtopping wave energy converters (OWECs), the overtopped wave flow directly affects power generation. Therefore, ongoing research is focused on the design parameters and configurations that influence wave flow and overall efficiency.

Previous studies have extensively explored these aspects. Kofoed **[1]** validated the effects of design parameters on wave energy converters through model experiments. Victor *et al.* **[2]** analyzed the impact of design scenario variations on overtopping efficiency and power generation. Jungrungruengtaworn *et al.* **[3]** conducted comparative analyses of overtopping performance through model experiments and numerical simulations, focusing on the inlet design parameters of multistage overtopping converters. De Barros *et al.* **[4]** examined the influence of attached substructures on the performance of wave energy converters. Cao *et al.* **[5]** revisited the governing equations for OWECs, and Da Silva *et al.* **[6]** applied a constructal design methodology to design and validate a novel wave energy converter.

This study investigated the effect of modifying the angle of the upper ramp of an OWEC on energy efficiency using computer simulations. The analysis environment was based on prior

† Corresponding Author (ORCID: https://orcid.org/0000-0001-9884-6650): Associate Professor, Division of Naval Architecture and Ocean Engineering, Gyeongsang National University, 2, Tongyeonghaean-ro, Tongyeong-si, 650-160, Korea, E-mail: gnujhlee@gnu.ac.kr, Tel: 055-772-9194

1 Ph. D. Candidate, Department of Ocean System Engineering, Gyeongsang National University, E-mail: tig01129@gnu.ac.kr, Tel: 055-772-9190

This is an Open Access article distributed under the terms of the Creative Commons Attribution Non-Commercial License (http://creativecommons.org/licenses/by-nc/3.0), which permits unrestricted non-commercial use, distribution, and reproduction in any medium, provided the original work is properly cited.

Copyright ⓒ The Korean Society of Marine Engineering

research by Kim *et al.* **[7]**, who analyzed coastal conditions in Ulleungdo, South Korea. The simulation was conducted using the particle-based computational fluid dynamics method and smoothed particle hydrodynamics (SPH), implemented in the DualSPHysics software. The upper ramp angle of the wave energy converter was treated as a design variable, and simulations were performed to assess the impact of ramp angle variations on the efficiency.

2. SPH Method

This section describes the SPH method used for the design and simulation of the OWEC. The kernel function and momentum equation used in the SPH approach are described in detail below.

2.1 Kernel Function

Fluid analysis methods are broadly divided into Eulerian methods, which analyze fluid flow within a fixed spatial framework, and Lagrangian methods, which represent fluids as particles characterized by physical properties such as mass, density, pressure, and velocity. The SPH method is a fluid analysis technique based on a Lagrangian framework. In SPH, the physical properties of fluid particles are calculated based on their interactions with neighboring particles. These interactions are approximated using a kernel function, as expressed in **Equation (1)**.

$$F(r) = \int F(r')W(r - r', h)dr' \tag{1}$$

Here, r represents the physical quantity of a particle, and r' represents the physical quantity of neighboring particles around r. The SPH method discretizes **Equation (1)** to obtain an approximate form, as shown in **Equation (2)**.

$$F(r_i) \approx \sum_j F(r_j)\frac{m_j}{\rho_j} W(r_i - r_j, h) \tag{2}$$

Here, $F(r_i)$ represents the physical quantity at particle r_i, and r_j denotes the individual particles surrounding particle r_i. m_j and ρ_j represent the mass and density of particle *j*, respectively. $W(r_i - r_j, h)$ is the kernel function, which is defined based on smoothing length h and the distance between particles *i* and *j*. The kernel function is expressed as

$$W(\mathbf{r}, h) = \alpha_D \begin{cases} 1 - \frac{3}{2}q^2 + \frac{3}{4}q^3 & 0 \le q \le 1 \\ \frac{1}{4}(2-q)^3 & 1 \le q \le 2 \\ 0 & q \ge 2 \end{cases} \tag{3}$$

In **Equation (3)**, r denotes the distance between particle *i* and its neighboring particle *j*, while $q = r/h$ represents the dimensionless distance between particles. The coefficient α_D is defined as $10/7\pi h^2$ for two-dimensional cases and $1/\pi h^3$ for three-dimensional cases.

2.2 Momentum Equation

In the SPH method, the motion of the fluid is described by the Navier–Stokes equations. The Navier–Stokes equation with respect to time t is given as

$$\frac{d\mathrm{v}}{dt} = -\frac{1}{\rho}\nabla P + g + v_0\nabla^2\mathrm{v} \tag{4}$$

Here, $-\frac{1}{\rho}\nabla P$ is the pressure, $v_0\nabla^2\mathrm{v}$ represents the viscous stress, and g denotes the gravitational acceleration. Artificial viscosity was applied to account for the viscous term that determines the fluid behavior in the Navier–Stokes equation. In this study, the artificial viscosity term proposed by Monaghan **[8]** was used and is expressed by the following equation:

$$\frac{d\mathrm{v_i}}{dt} = \sum_j m_j \left(\frac{P_j + P_i}{\rho_j \cdot \rho_i} + \prod_{ij}\right)\nabla_i W_{ij} + g \tag{5}$$

In **Equation (5)**, P and ρ represent the pressure and density at points *i* and *j*, respectively. The viscosity term $\prod_{ij}$ is defined as follows:

$$\prod_{ij} = \begin{cases} \frac{-\alpha\overline{c_{ij}}\mu_{ij}}{\overline{\rho_{ij}}} & v_{ij}\cdot \mathrm{r}_{ij} < 0 \\ 0 & v_{ij}\cdot \mathrm{r}_{ij} > 0 \end{cases} \tag{6}$$

Here, $\mathrm{r}_{ij} = r_i - r_j$ and $v_{ij} = v_i - v_j$ denote the position and velocity differences between particles *i* and *j*, respectively. $\overline{c_{ij}} = 0.5(c_i + c_j)$ represents the average speed of sound, and α is a constant set to 0.01. The term μ_{ij} in **Equation (6)** is given as follows:

$$\mu_{ij} = \frac{h v_{ij}\cdot \mathrm{r}_{ij}}{\mathrm{r}_{ij}^2 + \eta^2} \tag{7}$$

Here, η^2 is defined as the square of the smoothing length h, multiplied by 0.01.

In the SPH method, when analyzing incompressible fluids, the fluid is assumed to exhibit slight compressibility. The equation

of state representing this compressibility was proposed by Monaghan *et al.* **[9]** and is expressed as follows:

$$P = b\left[\left(\frac{\rho}{\rho_0}\right)^{\gamma} - 1\right] \tag{8}$$

In **Equation (8)**, $\gamma = 7$, $b = c_0^2\rho_0/\gamma$ and $\rho_0 = 1000kg/m^3$ represents the reference density. c_0 denotes the speed of sound at the reference density.

3. OWEC Model

3.1 Model Conditions

Ulleungdo was selected as the study area based on the reference by An *et al.* **[10]**. The simulation scaling factor was set to 1/20 of the actual sea conditions to accommodate future comparisons with physical model experiments and align with the dimensions of a two-dimensional wave flume. The environmental parameters used in this study are listed in **Table 1**.

Table 1: Wave conditions

	Wave conditions	
	1/1 scale	1/20 scale
Wave Height [m]	2.8	0.14
Wave Period [s]	7.37	1.65
Wave Length [m]	84.81	4.24
Water depth [m]	18	0.9

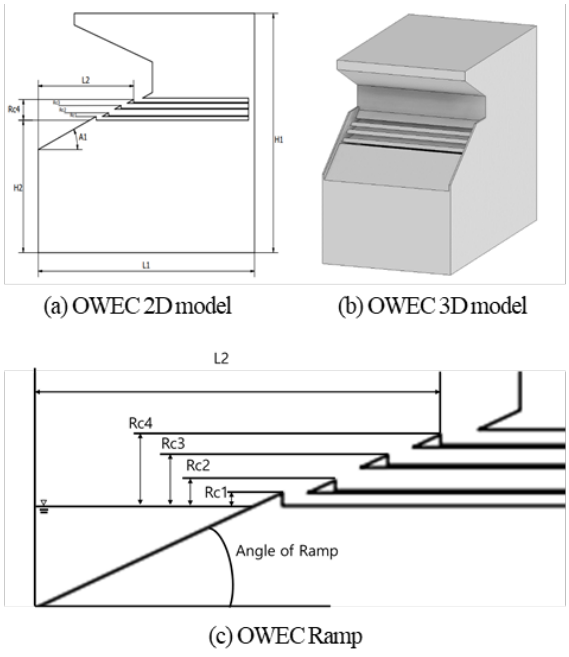

Figure 1: Geometry of overtopping wave energy converter (OWEC)

Table 2: Parameters of OWEC

Parameters	OWEC	Parameters	OWEC
Length of Bottom L1 [m]	3.6	Height of Reservoir Rc1 [m]	0.05
Length of Ramp L2 [m]	1.15	Height of Reservoir Rc2 [m]	0.1
Height of OWEC H1 [m]	3.25	Height of Reservoir Rc3 [m]	0.2
Water depth H2 [m]	1.8	Height of Reservoir Rc4 [m]	0.28
Angle of Ramp [°]	35	Reservoir slot w [m]	0.1

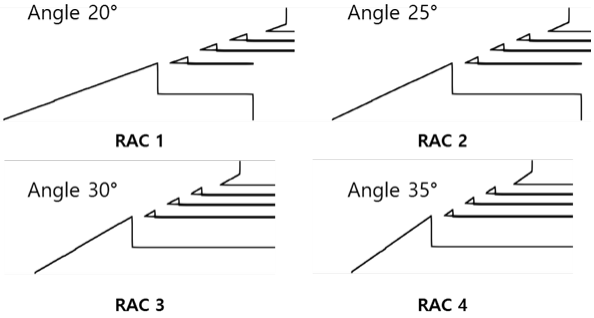

Figure 2: Designed models

Table 3: The parameters of change models

Parameters	Ramp Angle Change [RAC]			
	1	2	3	4
Height of Reservoir Rc1 [m]	0.05	0.05	0.05	0.05
Height of Reservoir Rc2 [m]	0.1	0.1	0.1	0.1
Height of Reservoir Rc3 [m]	0.2	0.2	0.2	0.2
Height of Reservoir Rc4 [m]	0.28	0.28	0.28	0.28
Reservoir slot w [m]	0.1	0.1	0.1	0.1
Angle of Ramp [°]	20	25	30	35

The model used in this study is identical to that used by An *et al.* **[10]**. The design and dimensions of the baseline model are illustrated in **Figure 1** and detailed in **Table 2**. The ramp angle of the upper structure of the wave energy converter was chosen as a design variable, with the angles varying incrementally from 20° to 35° at 5° intervals. The geometries and specifications of the modified models are shown in **Figure 2** and **Table 3**.

3.2 2D-numerical water tank

A two-dimensional numerical water tank was generated and analyzed using the SPH method. The environmental and numerical parameters of the two-dimensional water tank are illustrated in **Figure 3** and summarized in **Table 4**.

A piston-type wave generator with a distance of 4 m between the wave generator and structure and a water depth of 0.9 m was

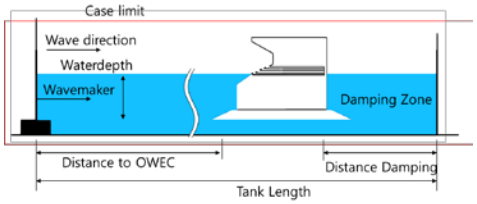

Figure 3: Geometry of 2D-numerical water tank

Table 4: Parameters of 2D-numerical water tank

Parameters	Water tank
Tank Length [m]	8
Distance to OWEC [m]	4
Distance Damping [m]	3
Water depth [m]	0.9
Wave maker type	Piston

employed. The motion of the piston-type wave generator is described as follows (Biesel and Suquet **[11]**):

$$e(t) = \frac{S_0}{2} sin(\omega t + \delta) \tag{9}$$

The wave generator moves according to its displacement $e(t)$ over time, where ω represents the wave frequency. δ is the initial phase, which is set to 0 in this study. S_0 denotes the stroke of the wave generator, which is related to the wave height H as expressed in **Equation (10)**.

$$\frac{H}{S_0} = \frac{2sinh^2(kd)}{sinh(kd)\,cosh(kd)+kd} \tag{10}$$

The wave frequency ω is determined using the dispersion relationship for shallow water, as shown in **Equation (11)**.

$$\omega^2 = gk\,tanh(kd) \tag{11}$$

where d represents the water depth, and k denotes the wave number.

4. Results

4.1 Hydraulic Efficiency

The performance of the OWEC was analyzed by comparing its overtopping flow rate and energy efficiency. In this study, we utilized hydraulic efficiency, which represents the energy efficiency related to overtopping, as proposed by Margheritini *et al.* **[12]**. The equation for the hydraulic efficiency is as follows:

$$\eta_{hyd} = \frac{P_{crest}}{P_{wave}} \tag{9}$$

where P_{crest} denotes the potential energy of the overtopped fluid. For a multistage OWEC, this is expressed as the sum of the potential energies of the fluid overtopped into each reservoir.

$$P_{crest} = \sum_{j=1}^{n} \rho g q_j R_{c,j} \tag{10}$$

In this equation, ρ is the density of the fluid, g is the gravitational acceleration, q_j represents the overtopping flow rate into the j-th reservoir, and $R_{c,j}$ is the height from the sea level to the inlet of the j-th reservoir. The flow rate was measured based on the wave period used in the analysis, and the average value was adopted. P_{wave} represents the kinetic energy of the incident wave approaching the OWEC.

$$P_{wave} = \frac{1}{16}\rho g H^2 c \left[1 + \frac{2kd}{sinh(kd)}\right] \tag{11}$$

where c is the phase velocity of the wave, H is the wave height, d is the water depth, and k is the number of waves.

4.2 Analysis Results

This study aims to analyze the differences in hydraulic efficiency according to changes in the ramp angle of an OWEC. The analysis results for the models with varying ramp angles are presented in **Table 5** and **Figure 4** and **Figure 5**. Additionally, **Figure 6** illustrates the flow process in each reservoir over a single-wave period. **Figure 6** shows that the overtopped waves enter the reservoir through two processes: ascending along the ramp and descending along the ramp.

Figure 4 shows the hydraulic efficiency of each reservoir in the models, and **Figure 5** highlights the trend in the overtopping efficiency of each reservoir. As shown in **Table 5**, the hydraulic efficiencies of the models ranges from 30% to 37%. Overall hydraulic efficiency is highest in RAC 4, and it increases with ramp angles. Examining the changes in hydraulic efficiency by stage reveals that the efficiency of the 1st and 2nd reservoirs increases as the ramp angle becomes steeper, while the hydraulic efficiency of the 3rd and 4th reservoirs decreases with increasing ramp angle.

Although RAC 1 exhibits the lowest overall hydraulic efficiency, it demonstrates the highest hydraulic efficiency at the 4th reservoir inlet among the four models. **Figure 6** shows that in the RAC 1 model, the wave's kinetic energy in the direction of the structure is transmitted along the ramp to the 4th reservoir inlet. For RAC 1, waves primarily enter the reservoir during the ascending motion. The RAC 2 model shows a similar trend to RAC 1.

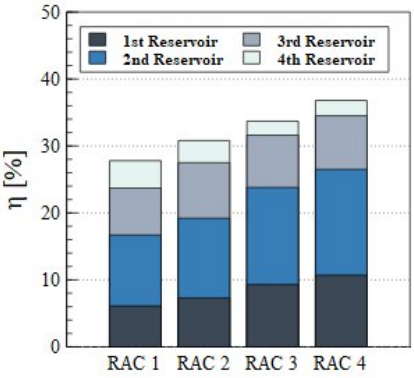

Figure 4: Hydraulic efficiency distribution across model

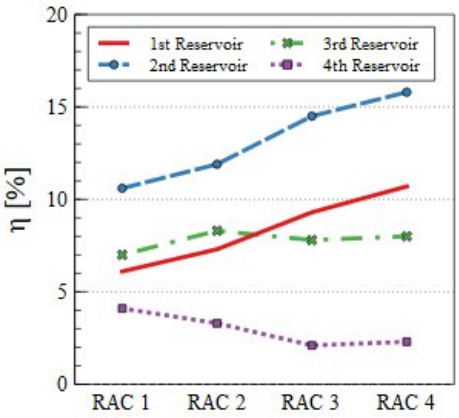

Figure 5: Hydraulic efficiency for each reservoir

Table 5: Hydraulic efficiency of models

Model	$\eta_{hyd},1$	$\eta_{hyd},2$	$\eta_{hyd},3$	$\eta_{hyd},4$	η_{hyd},all
RAC 1	0.061	0.106	0.07	0.041	0.278
RAC 2	0.073	0.119	0.083	0.033	0.308
RAC 3	0.093	0.145	0.078	0.021	0.337
RAC 4	0.107	0.158	0.08	0.023	0.368

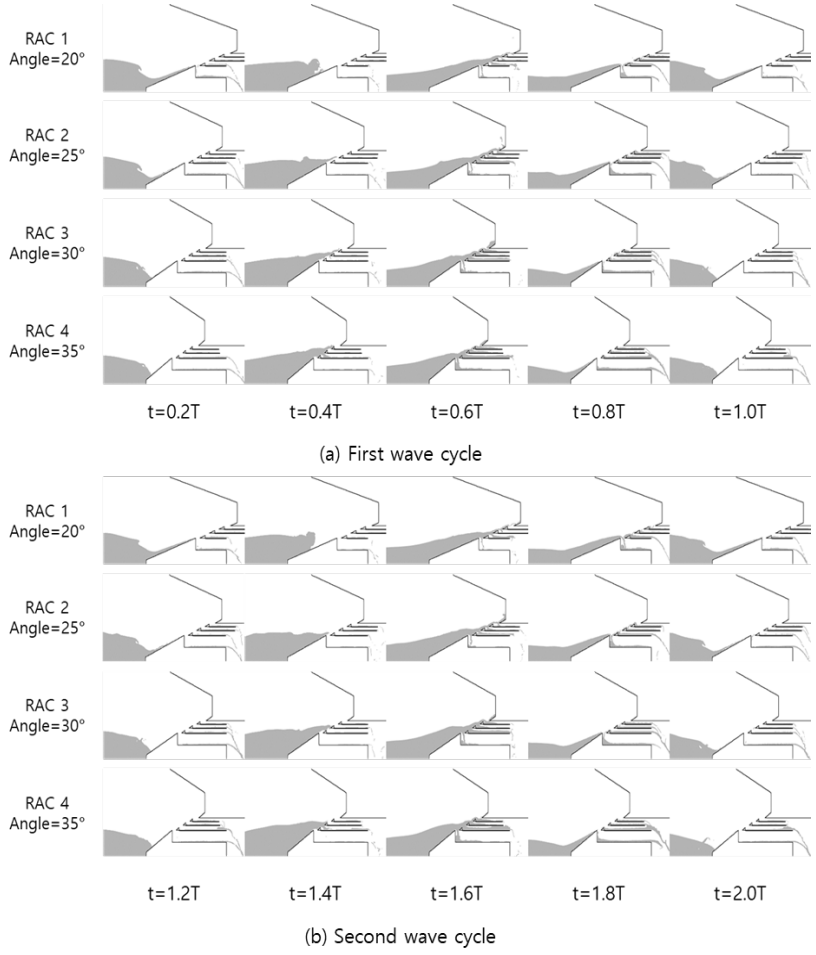

Figure 6: Overtopping motion

For RAC 3 and RAC 4 models with ramp angles of 30° or higher, most of the hydraulic efficiency was concentrated in the 1st and 2nd reservoirs. As shown in **Figure 6**, the overtopping waves in RAC 3 and RAC 4 ascend along the ramp to the 4th reservoir inlet. However, owing to the steep angles, more wave energy enters the reservoirs during the descending motion than during the ascending motion. This indicates that as the ramp angle increases, the descending waves have a greater influence on hydraulic efficiency.

The analysis results indicate that the RAC 4, with a ramp angle of 35 degrees, demonstrated the highest performance in the simulation domain. This superior performance is attributed to the increased ramp angle, which effectively concentrated wave energy into the 1st and 2nd reservoirs, maximizing energy efficiency. Notably, the steeper angle enhanced the descending wave motion, resulting in an increased inflow of water into the reservoirs. Conversely, the efficiency of the 3rd and 4th reservoirs decreased as the ramp angle increased. However, the high efficiency of the first and second reservoirs offset this decline, leading to an overall improvement in performance.

5. Conclusion

This study investigated the effect of ramp-angle variations on the energy efficiency of an OWEC. The simulation results demonstrated that the ramp angle significantly influenced a critical role in determining the hydraulic efficiency and energy distribution within the reservoirs.

As the ramp angle increased, the hydraulic efficiencies of the 1st and 2nd reservoirs showed an upward trend, whereas those of the 3rd and 4th reservoirs decreased. These findings suggest that steeper angles favor the wave energy contribution during the descending motion rather than during the ascending motion. Notably, models with ramp angles of 30° or greater exhibited most of their hydraulic efficiencies in the 1st and 2nd reservoirs.

In conclusion, the ramp angle design is a key parameter for optimizing the performance of OWECs. However, this study is based on two-dimensional simulation results. Further research involving three-dimensional simulations of the OWEC geometry is required for performance analysis, as well as model experiments to ensure the reliability of the simulation results. Additionally, the environmental conditions used in this study involved regular waves, which differ from actual conditions. Future studies should incorporate irregular waves that reflect real-world environmental conditions.

Acknowledgement

This work was supported by National R&D Program through the National Research Foundation of Korea (NRF) funded by the Korea government (Ministry of Science and ICT) (No. 2021R1I1A3057230).

Author Contributions

Conceptualization, S.-H. An and J.-H. Lee; Methodology, S.-H. An; Software, S.-H. An; Validation, S.-H. An and J.-H. Lee; Formal Analysis, S.-H. An; Investigation, S.-H. An; Resources, S.-H. An; Data Curation, S.-H. An; Writing—Original Draft Preparation, S.-H. An; Writing—Review & Editing, J.-H. Lee; Visualization, S.-H. An; Supervision, J.-H. Lee; Project Administration, J.-H. Lee; Funding Acquisition, J.-H. Lee.

References

[1] J. P. Kofoed, Wave Overtopping of Marine Structures Utilization of Wave Energy, Ph. D. Dissertation, Aalborg University, Aalborg, Denmark, 2002.

[2] L. Victor, P. Troch, and J. P. Kofoed, “On the effects of geometry control on the performance of overtopping wave energy converters,” Energies, vol. 4, no. 10, pp. 1574-1600, 2011.

[3] S. Jungrungruengtaworn, R. Reabroy, N. Thaweewat, and B. S. Hyun, “Numerical and experimental study on hydrodynamic performance of multi-level OWEC,” Ocean Systems Engineering, vol. 10, no. 4, pp. 359-371, 2020.

[4] A. S. De Barros, C. Fragassa, M. D. S. Paiva, L. A. Rocha, B. N. Machado, L. A. Isoldi, and E. D. dos Santos, “Numerical study and geometrical investigation of an onshore overtopping device wave energy converter with a seabed coupled structure,” Journal of Marine Science and Engineering, vol. 11, no. 2, 412, 2023.

[5] D. Cao, J. He, and H. Chen, “Empirical predictions on wave overtopping for overtopping wave energy converters: a systematic review,” Processes, vol. 12, no. 9, 1940, 2024.

[6] S. A. Da Silva, J. C. Martins, E. D. dos Santos, L. A. O. Rocha, B. N. Machado, L. A. Isoldi, and M. das Neves Gomes, “Constructal design applied to an overtopping wave energy converter locate on Paraná Coast in Brazil,” Sustainable Marine Structures, vol. 6, no. 2, pp. 1-14, 2024.

[7] G. G. Kim, S. H. An, and J. H. Lee, “Review of the optimal locations of coastal sea area for operating wave energy converter in Korea,” Journal of Advanced Marine Engineering and Technology, vol. 46, no. 4, pp. 172-181, 2022.

[8] J. J. Monaghan, “Smoothed particle hydrodynamics,” Annual Review of Astronomy and Astrophysics, vol. 30, pp. 543-574. 1992.

[9] J. J. Monaghan, R. A. Cas, A. M. Kos, and M. Hallworth, “Gravity currents descending a ramp in a stratified tank,” Journal of Fluid Mechanics, vol. 379, pp. 39-69, 1999.

[10] S. H. An, J. H. Lee, G. G. Kim, and D. H. Kang, “Optimal design of overtopping wave energy converter substructure based on smoothed particle hydrodynamics and structural analysis,” Journal of the Korean Society of Marine Environment & Safety, vol. 29, no. 7, pp. 992-1001, 2023.

[11] F. Biesel and F. Suquet, “Etude theorique d'un type d'appareil a la houle. La Houille Blanche,” vol. 6, no.2, pp. 152-165, 1951.

[12] L. Margheritini, D. Vicinanza, and P. Frigaard, “SSG wave energy converter: Design, reliability and hydraulic performance of an innovative overtopping device,” Renewable Energy, vol. 34, no. 5, pp. 1371-1380, 2009.